Search for the η_c' $(2\,^1S_0)$ charmonium resonance

M. Ambrogiani,[2] S. Argirò,[6] S. Bagnasco,[6] W. Baldini,[2] D. Bettoni,[2] G. Borreani,[6] A. Buzzo,[3] R. Calabrese,[2] R. Cester,[6] P. Dalpiaz,[2] G. Garzoglio,[1] K. E. Gollwitzer,[4] A. Hahn,[1] S. Jin,[5] J. Kasper,[5] G. Lasio,[4] M. Lo Vetere,[3] E. Luppi,[2] P. Maas,[5] M. Macrì,[3] M. Mandelkern,[4] F. Marchetto,[6] M. Marinelli,[3] W. Marsh,[1] M. Martini,[2] E. Menichetti,[6] R. Mussa,[2] M. M. Obertino,[6] M. Pallavicini,[3] N. Pastrone,[6] C. Patrignani,[3] J. Peoples Jr.,[1] S. Pordes,[1] E. Robutti,[3] J. Rosen,[5] P. Rumerio,[6] A. Santroni,[3] M. Savrié,[2] J. Schultz,[4] G. Stancari,[2] M. Stancari,[4] J. Streets,[1] S. Werkema,[1] and G. Zioulas[4]

(E835 Collaboration)

[1]*Fermi National Accelerator Laboratory, Batavia, Illinois 60510*
[2]*Istituto Nazionale di Fisica Nucleare and University of Ferrara, 44100 Ferrara, Italy*
[3]*Istituto Nazionale di Fisica Nucleare and University of Genova, 16146 Genova, Italy*
[4]*University of California at Irvine, California 92697*
[5]*Northwestern University, Evanston, Illinois 60208*
[6]*Istituto Nazionale di Fisica Nucleare and University of Torino, 10125 Torino, Italy*

(Received 18 January 2001; published 10 August 2001)

We report on a search by Fermilab experiment E835 for the η_c' $(2\,^1S_0)$ charmonium resonance in the process $\bar{p}p \to \eta_c' \to \gamma\gamma$. No signal was observed and, based on 34 pb^{-1} integrated luminosity, we determine the following upper limits (90% confidence level) to the product of the branching ratios for a resonance mass in the region 3575–3660 MeV/c^2: $Br(\eta_c' \to \bar{p}p) \times Br(\eta_c' \to \gamma\gamma) < 12.0 \times 10^{-8}$ for $\Gamma = 5$ MeV; $< 5.9 \times 10^{-8}$ for $\Gamma = 10$ MeV; $< 4.8 \times 10^{-8}$ for $\Gamma = 15$ MeV. Combining the present data with those of the predecessor experiment, E760, the upper limits become 8.0×10^{-8}, 5.0×10^{-8}, and 4.5×10^{-8}, respectively. In the restricted region 3589–3599 MeV/c^2, where a candidate was reported by the Crystal Ball experiment, we obtain the following limits from the combined E760–E835 experiments: $Br(\eta_c' \to \bar{p}p) \times Br(\eta_c' \to \gamma\gamma) < 5.6 \times 10^{-8}$ for $\Gamma = 5$ MeV; $< 3.7 \times 10^{-8}$ for $\Gamma = 8$ MeV. A comparison of these with other experimental results is presented.

DOI: 10.1103/PhysRevD.64.052003 PACS number(s): 14.40.Gx, 13.40.Hq, 13.75.Cs

I. INTRODUCTION

The quark model, and its explicit formulation in terms of QCD, can explain many of the gross features of the spectrum and interactions of hadrons. A major step forward in the investigation of the role of QCD as the basis of the strong interactions would be the complete experimental determination of the energy levels and rates of the principal decays of the low lying states of quarkonium systems. The two best candidate systems for this are charmonium and bottomonium, and, of the two, the charmed quark-antiquark system has the lowest lying levels more fully mapped. Of the lowest charmonium states with radial quantum number $n = 1$ and 2, up to the $\psi'(2\,^3S_1)$, the Particle Data Group [1] currently lists only two states as needing confirmation: the singlet spin states $h_c(1\,^1P_1)$ and $\eta_c'(2\,^1S_0)$.

The singlet states of quarkonium are in general difficult to study, because they cannot be formed in e^+e^- annihilation nor can they result from electric dipole radiative decay of the triplet spin states formed in such annihilation. On the other hand, states of these quantum numbers, and indeed all states of quarkonium, can be resonantly produced in proton antiproton annihilations.

This paper reports on a search for the η_c', performed in the formation process

$$\bar{p}p \to \eta_c' \to \gamma\gamma \tag{1}$$

by Fermilab experiment E835, an upgraded continuation of experiment E760. As of this time, only one observation of this resonance was reported [2], but after many years this candidate still awaits confirmation.

II. EXPERIMENTAL METHOD

A. Technique

The Fermilab experiment E835 is devoted to the study of charmonium spectroscopy by direct formation of $c\bar{c}$ states in $\bar{p}p$ annihilation at the Fermilab Antiproton Accumulator ring [3]. A cylindrical jet of clusterized hydrogen molecules (6 mm diameter, $\rho_{max} \sim 3.0 \times 10^{14}$ atoms/cm^3) [4] intersects a beam of up to 80 mA of antiprotons ($\sim 8 \times 10^{11}$ stored particles) circulating in the accumulator to produce instantaneous luminosities of up to 5×10^{31} cm^{-2} s^{-1}. The resulting interaction region is $0.6 \times 0.6 \times 0.6$ cm^3. The jet target-detector setup is shown in Fig. 1. The density of the jet can be increased automatically to keep the instantaneous luminosity constant as the circulating antiproton beam intensity decreases.

The antiproton beam is stochastically cooled such that the rms spread in the center of mass energy $\sqrt{s}$, is ~ 0.35 MeV. The uncertainty in the mean center of mass energy at any energy point for these data is estimated to be ~ 0.2 MeV. The $c\bar{c}$ resonance parameters are determined precisely by measuring the excitation curve obtained by stepping the energy of the antiproton beam across the resonance; since the $c\bar{c}$ state is formed directly from the $\bar{p}p$ annihilation, the precision of the mass and width determination does not depend on

 ©2001 The American Physical Society

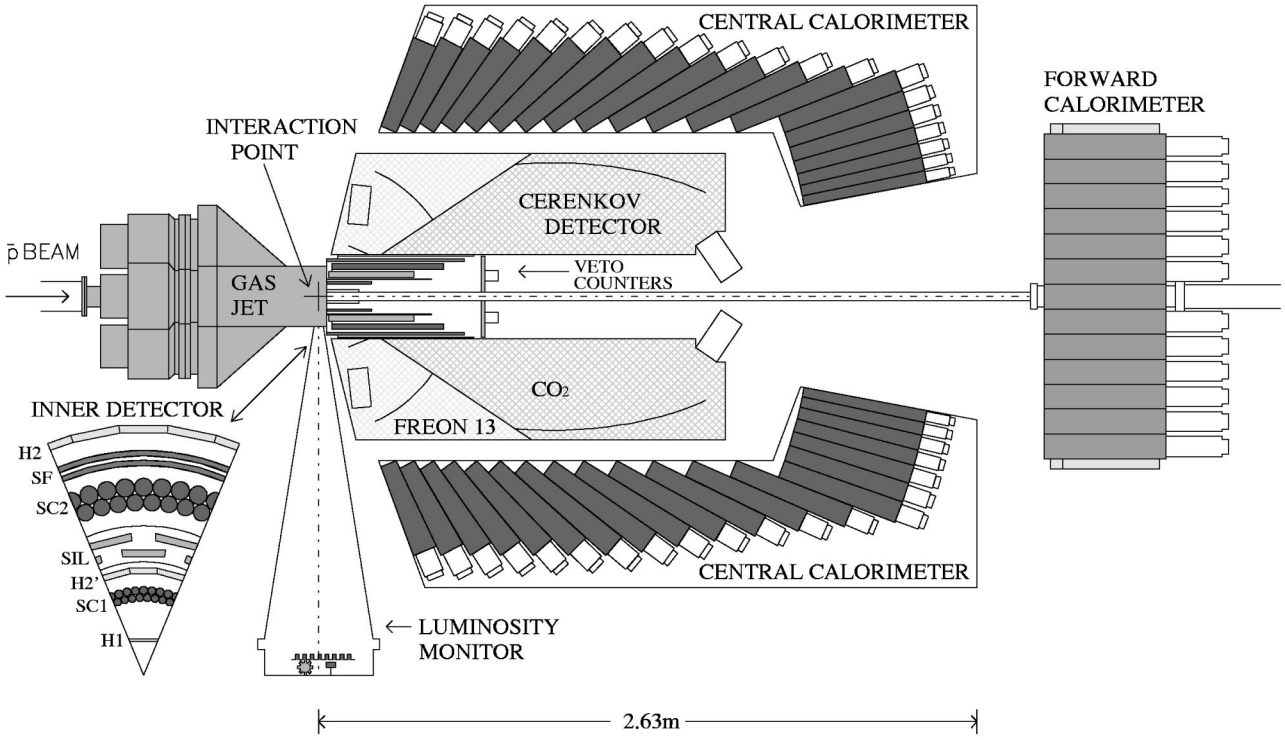

FIG. 1. E835 detector layout.

the resolution of the detector system but is determined only by event statistics and the knowledge of the antiproton beam energy and energy spread.

B. Detector

We select electromagnetic final states as tags of charmonium formation. This makes it possible to extract a clean signal despite the large hadronic background. The detector, shown in Fig. 1, is optimized for the selection of photons and electrons. It has full coverage in azimuthal angle (ϕ), and consists of a cylindrical central detector and a planar forward system.[1]

The central detector contains three azimuthally segmented scintillator hodoscopes identified as H1, H2′, and H2; two sets of straw tubes [5] for tracking in azimuth, a scintillating-fiber system [6] for tracking in polar angle (θ); a 16 cell threshold gas Čerenkov counter [7] for electron identification, and a 1280 element [20 rings (θ), each comprised of 64 counters (ϕ)] lead-glass central calorimeter (CCAL) [8] for measuring the directions and energies of photons and electrons. The CCAL covers polar angles $11° < \theta < 70°$ and measures the energy with a resolution given by the formula $\sigma(E)/E = 6\%/\sqrt{E(\mathrm{GeV})} + 1.4\%$. Coupled with the known position and dimension of the interaction region,[2] it provides a measurement of the polar and azimuthal angles with a resolution $\sigma_\theta = 6$ mrad and $\sigma_\phi = 11$ mrad, respectively.

The forward system includes an eight segment scintillator hodoscope (FCV) giving full coverage in ϕ in the polar region $2° < \theta < 10°$ and a forward electromagnetic calorimeter composed of 144 lead glass elements covering the region $3.3° < \theta < 11°$.

All counters are equipped with both time and pulse-height readout. The time measurements allow the rejection of signals from out-of-time events (accidental pileup).

A luminosity monitor [9] provides an absolute luminosity measurement with a statistical precision of better than 0.1% and an estimated systematic error of $\pm 2.5\%$, by measuring $\bar{p}p$ forward elastic scattering through the detection of proton recoils at $\sim 86.5°$ in three solid state detectors.

C. Trigger

The data used in the present analysis were collected at instantaneous luminosities ranging from ~ 1.5 to 2.5×10^{31} $\mathrm{cm}^{-2}\,\mathrm{s}^{-1}$, corresponding to an interaction rate of up to 1.5 MHz in the region of energy covered. Events of interest are selected by a fast hardware trigger (level-one), which reduces the rate to <2.5 kHz, and then is transferred to a set of processors where a software filter (level-two) is applied be-

[1]The axis of the central detector is along the antiproton beam and is taken as the polar axis to define θ and ϕ, the polar and azimuthal angles.

[2]The coordinates of the center of the interaction region are monitored on a stack by stack basis using the copious sample of kinematically determined $\bar{p}p \to \pi^0\pi^0 \to 4\gamma$ annihilations.

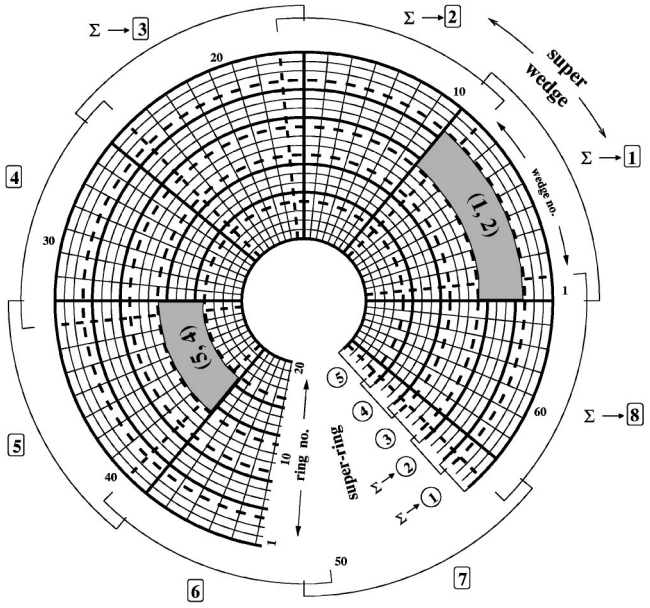

FIG. 2. A polar diagram of the central calorimeter showing the structure of the 40 supermodules which are arranged in an 8 (super-wedges) × 5 (super-rings) array. The overlaps are indicated by the thick (solid and dashed) lines. The shaded areas are an example of two hypothetical hits in supermodules (1-2) and (5-4).

fore recording the events on tape [10]. The level-one trigger accepts in parallel, final states containing either an electron and positron ($a1$) or two photons ($a2$) of large invariant mass; all neutral final states, where $\geqslant$80% of the initial state energy is contained in the central calorimeter (b). A random gate trigger is generated with a pulser operating between 1 and 10 Hz to obtain data used to study pileup.

The element common to the $a1$ and $a2$ triggers is an algorithm applied to the central calorimeter signals that is tailored to accept high mass e^+e^- and $\gamma\gamma$ final states with full efficiency [11]. The trigger requires the presence of two energy depositions with energy above a θ-dependent threshold and approximately coplanar with the $\bar{p}$ direction. It is implemented as follows. To reduce the number of signals to a manageable level, while maintaining the requirement for a concentrated energy deposition, the analog signals from the individual counters are summed to produce a matrix of 40 supermodules (8 in ϕ by 5 in θ), with appropriate overlap to ensure that 95% of the energy from an individual photon or electron is contained within one supermodule (see Fig. 2 for an illustration of the supermodules). The reduction is performed in two stages, from 1280 to 160 signals, and then from 160 to 40. In the first, signals from groups of 9 adjacent counters (same θ) are added to form 8 octants, with one counter overlap, for each of the 20 θ values. In the second, the resulting 160 signals (8 in ϕ by 20 in θ) are combined into weighted sums over θ in groups of 4 or 5, again allowing for overlap. The 40 analog signals from the supermodules are integrated and discriminated. The thresholds are set to $\sim$60% of the energies for a two-body reaction. This loose requirement also allows the detection of inclusive decays to a lower mass charmonium state (J/ψ or η_c). The discriminator outputs from the 5 supermodules in each octant are input to a logic or to form the 8 logic signals used for triggering.

To select events of type $a2$, corresponding to the signal sought in this investigation, we impose a coplanarity condition by requiring that two of the CCAL logic signals come from directly opposing octants (PBG1). We demand that no charged particles be detected in the final state, by requiring the charged veto to be off; the charged veto is on if there is at least one signal in the FCV or at least one hit above threshold in both a H1 element and one of the three corresponding H2′ elements. These counter systems together fully cover the polar angle range $2° \leqslant \theta \leqslant 65°$ over the complete azimuth.

To select events of type b, we sum the pulse heights from the entire central calorimeter, excluding the two rings with the smallest θ values, for an angular acceptance of $13° \leqslant \theta \leqslant 70°$. The total energy condition (ETOT) is met if the sum pulse exceeds a threshold corresponding to 80% of the initial state energy. For b, we require that the charged veto be off.

In the software trigger, we convert the CCAL pulse heights to energies, determine cluster coordinates and energies, and calculate the invariant masses of all pairs of clusters. All events for which any two CCAL clusters have invariant mass $\geqslant$2.2 GeV/c^2 are recorded and constitute the data set for this experiment. The clustering algorithm used on-line is a simplified version of the one used in the off-line analysis [12].

In the off-line analysis, a cluster consists of a 3×3 grid of counters containing $>$20 MeV centered on a block containing $>$5 MeV.

D. Data collection

The data were recorded in the 1996–1997 Fermilab fixed target run. Data were taken in the interval 3575 MeV$<\sqrt{s}<$3660 MeV to search the η_c' and at the η_c, J/ψ, χ_{c0}, χ_{c2}, ψ' and h_c ($\sim$3526 MeV, near the center of gravity of the three χ states). The data used for this analysis are summarized in Table I. The integrated luminosity for this search is 34.1 pb^{-1} plus additional luminosity used for background determination.

III. DATA ANALYSIS

A. Cluster timing

The most important element of the upgrade from E760 to E835 is the addition of pulse shaping to the Central Calorimeter signals and time to digital converters (TDCs) to nearly every detector in the apparatus. This upgrade was motivated by the significantly greater instantaneous luminosity available to E835 and is particularly important for low signal, high background channels such as $\gamma\gamma$, where extra hits from out of time events can cause good events to be rejected. For CCAL, TDC information is present with nearly unit efficiency for clusters with energies $>$75 MeV. The efficiency falls to $\sim$0.5 at 30 MeV and to zero at $\sim$20 MeV. The data for all the counters in a cluster are corrected for slewing [13] and referred to a time derived from the analog signals from the first stage of summing of CCAL. For each cluster we consider the counters with the two largest numbers of analog

TABLE I. Summary of the data for the η_c' search; $\sigma_{\sqrt{s}}$ is the standard deviation of the center of mass energy distribution due to the energy spread of the antiproton beam, n is the number of candidate events with $\cos\theta^* \leq 0.4$, and $\epsilon_{\gamma\gamma}$ is the combined trigger and analysis efficiency.

$\sqrt{s}$ (MeV)	$\int \mathcal{L}\, dt$ (pb^{-1})	$\sigma_{\sqrt{s}}$ (MeV)	n	$\epsilon_{\gamma\gamma}$
3526.08	46.649	0.300	664	0.749
3535.45	1.304	0.533	15	0.751
3544.79	0.998	0.253	8	0.814
3576.05	1.606	0.251	23	0.752
3580.49	1.210	0.339	23	0.750
3585.19	1.506	0.358	18	0.748
3590.25	1.484	0.356	24	0.777
3595.62	1.507	0.336	21	0.764
3600.50	1.594	0.354	24	0.780
3604.00	1.479	0.271	21	0.781
3607.53	1.524	0.361	14	0.741
3610.58	0.922	0.419	6	0.779
3614.71	1.538	0.314	32	0.757
3620.59	1.472	0.353	21	0.780
3625.30	1.637	0.307	22	0.755
3629.75	1.619	0.366	16	0.773
3633.43	4.587	0.335	45	0.715
3635.17	1.408	0.371	21	0.747
3639.98	1.498	0.437	26	0.732
3643.95	2.956	0.337	43	0.767
3651.63	1.456	0.288	11	0.749
3656.07	1.646	0.333	12	0.751
3660.48	1.486	0.391	20	0.752
3686.24	8.011	0.378	75	0.630

to digital converters (ADCs) counts. If neither has TDC information, the cluster is identified as *undetermined*. If either has a corrected time within 10 ns of the reference time, the cluster is identified as *in-time*. The cluster is otherwise identified as *out-of-time*.

B. $\gamma\gamma$ event selection

Event selection is optimized to select $\gamma\gamma$ candidates with high efficiency while reducing the background from $\pi^0\pi^0$ and $\pi^0\gamma$ final states to an acceptable level. These candidate events satisfy the $a2$ or b trigger. In a preliminary selection, we require the largest two-cluster invariant mass to be within 20% of $\sqrt{s}$ and the corresponding CCAL clusters to satisfy $15° < \theta < 60°$. A more stringent selection is imposed subsequently: a four constraint kinematical fit to the hypothesis $\bar{p}p \to \gamma\gamma$ is performed using the SQUAW program [14], and the events with a nominal confidence level below 5% are discarded.

Events containing symmetrically-decaying π^0s are readily distinguished from $\gamma\gamma$ events [12]. A small fraction of the abundant $\pi^0\pi^0$ and $\pi^0\gamma$ events satisfy the selection when the π^0(s) decays highly asymmetrically. Further cuts are imposed to reduce this background. No in-time extra clusters in CCAL are allowed in the candidate events. Out-of-time extra clusters are disregarded and all undetermined extra clusters are paired with each candidate photon and the event is rejected if the invariant mass of any pair falls within 35 MeV/c^2 of the π^0 mass (135 MeV/c^2). In some asymmetric decays, the low energy photon escapes detection because it is below the energy threshold or is not contained in the angular acceptance of CCAL. This background can be reduced by exploiting the difference between the angular distribution of the signal being sought, which is isotropic, and that of the background; the $\pi^0\pi^0$ and $\pi^0\gamma$ angular distributions are strongly peaked in the forward direction leading to a forward-peaked $\gamma\gamma$ background distribution. By restricting the acceptance to a region of the center of mass angle θ^* near 90° we can increase the signal background ratio at the expense of signal events. An optimal acceptance cut must be chosen, $\cos\theta^* < \alpha$, to maximize the significance of the signal. We determine α *a priori*, as described in the Appendix of Ref. [15]. This method maximizes the power for discrimination between the resonance and the pure background hypotheses. We find that the optimal value of α in the η_c' region is approximately 0.40 and we choose $\alpha = 0.4$, even though the apparatus acceptance extends up to 0.55.

We observe no evidence for contamination by η inclusive events [15].

In general, an inefficiency in the charged veto will allow high mass e^+e^- events to enter the sample. This effect is completely negligible everywhere except at the ψ' formation energy, where there is a significant source of such events from ψ' exclusive decays to e^+e^-. To reduce the contamination to the required level (<0.5 event/pb^{-1}) we excluded a 27.5° region of azimuthal angle, and the azimuthal region opposite it, because of a known inefficiency in the charged veto in that region. This cut was applied only to the ψ' data, to avoid extending the ensuing 15% loss of efficiency to the whole data sample.

The event totals, for the selection described above, are tabulated in Table I.

C. Efficiency and acceptance determination

The overall efficiency for the $\gamma\gamma$ channel is

$$\epsilon_{\gamma\gamma} \equiv \epsilon_1 \times (1 - P_{conv})^2 \times (1 - P_{cont}) \times \epsilon_2 . \qquad (2)$$

ϵ_1 is the efficiency of generating either the PBG1 or the ETOT signals, P_{conv} is the probability that a photon converts in the material before the first detector element, P_{cont} is the probability that an accidental event contaminates a signal event, and ϵ_2 is substantially the efficiency of the kinematic fit.

ϵ_1 is $\sim 100\%$ and is measured by exploiting the fact that CCAL has the same response to high energy photons as to electrons. A sample of $\bar{p}p \to J/\psi \to e^+e^-$ events was selected with a special trigger not requiring either PBG1 or ETOT. The efficiency of the PBG1 signal was found to be $>99.99\%$; the efficiency of the ETOT signal was found to be $>99.8\%$.

P_{conv} is the probability that a photon converts into an e^+e^- pair before reaching the first detector element (H1),

thus setting the charged veto. Calculation of the probability of conversion in the 0.14 mm stainless steel beam pipe, averaged over the angular distribution of the $\gamma\gamma$ events, gives a value $P_{conv}=0.011\pm0.001$.

P_{cont} is the probability that a random event contaminates a good event, causing it to be rejected.[3] This can happen at the trigger level if the overlapping event sets the charged veto, or in the off-line analysis if (a) the second event occurs within ~10 ns of a real $\gamma\gamma$ event and contributes one or more *in-time* clusters in CCAL, or if (b) one time-*undetermined* cluster from the overlapping event forms the π^0 mass when combined with a photon from the $\gamma\gamma$ event.

ϵ_2 is predominantly the efficiency of the kinematic fit,[4] but also incorporates small localized inefficiencies not accounted for in ϵ_1 and originating from a few dead CCAL channels.

P_{cont} and ϵ_2 are determined together for each data point by Monte Carlo techniques. The Monte Carlo program simulates the CCAL response to $\bar{p}p\to\gamma\gamma$ events starting from the energy deposited in each counter, taking account of passive material and dead channels (typically 4 out of 1280). The effect of accidental events is incorporated by superimposing (actual) data taken with a random gate on the simulated events. The combined events are subject to the standard clustering algorithms and analysis cuts, and the quantity $(1-P_{cont})\times\epsilon_2$ is given by the fraction which survive.

The factor $(1-P_{cont})$ varies linearly from ~0.88 at $\mathcal{L}\sim1.5\times10^{31}$ cm^{-2} s^{-1} to ~0.81 at $\mathcal{L}\sim2.5\times10^{31}$ cm^{-2} s^{-1}, the luminosity range for these data; ϵ_2 is typically 90%. Given that we use actual data events to simulate the contamination, we estimate less than 1% systematic error in $(1-P_{cont})$. The uncertainty of ϵ_2 was determined from a sample of real $J/\psi\to e^+e^-$ events. These events can be selected with high efficiency and free of background without using the kinematical fit, thus permitting a direct measurement of ϵ_2 to be compared with the Monte Carlo calculation. We found $\epsilon_{2_{MC}}-\epsilon_{2_{exp}}=0.002\pm0.025$.

The overall efficiency for each data point is calculated using Eq. (2). Its values are reported in Table I. They have an estimated relative error at most ~3%, calculated by adding in quadrature the contributions from the maximal errors on P_{cont} and ϵ_2, and the error on P_{conv}.

Since the two photon decay of the η_c' is isotropic, the geometrical acceptance is equal to the $|\cos\theta^*|$ cutoff value $\alpha=0.4$.

IV. RESULTS

A. E835 experiment

The cross section measurements for candidate $\gamma\gamma$ events within the acceptance region ($\cos\theta^*<0.40$) obtained from data taken at various center of mass energies between 3526 and 3686 MeV are shown as open circles in Fig. 3. Data taken at 3556.2 MeV, where a $\chi_{c2}\to\gamma\gamma$ signal was observed [15], have been excluded, since they are not used in this paper. Cross sections have been corrected for analysis and trigger inefficiencies. No resonance signal is seen in the plot. The full circles refer to our previous experiment E760 and will be discussed in Sec. IV B.

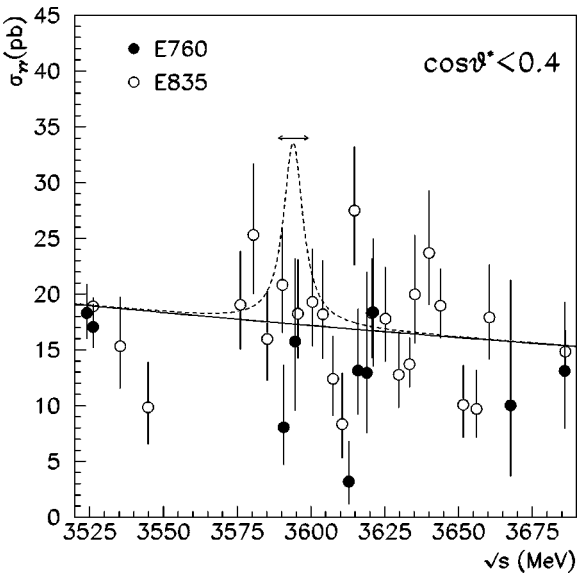

FIG. 3. Cross section for $\bar{p}p\to\gamma\gamma$ candidates vs center of mass energy: open and full circles for E835 and E760, respectively. The fact that the background levels in the two experiments differ is accounted for in the analysis (see the text). The dashed line shows, superimposed on the E835 best fit background, an estimate of the signal expected for an η_c' candidate with an assumed width of 8 MeV. The uncertainty on the estimated peak cross section is 40% ignoring the theoretical uncertainty (see the text). The signal is drawn at the mass of the crystal ball η_c' candidate with the uncertainty in its mass indicated by the overlaying horizontal segment.

The background to the resonance search consists of a continuum two photon production (expected to be very small[5]) and a fraction of $\pi^0\pi^0$ and $\pi^0\gamma$ events that survive the event selection. These processes are expected to produce a background with smooth energy dependence. We describe the background with the form

$$\sigma_{bkgd}(s)=A\left(\frac{3556.2\ \text{MeV}}{\sqrt{s}}\right)^B \tag{3}$$

and use high integrated luminosity data points at ~3526 and 3686 MeV (46.6 pb^{-1} and 8 pb^{-1}, respectively) to help constrain the background level throughout the search region.

[3]Since the $\bar{p}$ beam has no time structure, this probability follows Poisson statistics and is determined by the interaction rate.

[4]The inefficiency is almost twice that expected from the theoretical χ^2 distribution, due to non-Gaussian tails of the error distributions.

[5]In spite of the small cross section, possible interference of the nonresonant continuum $\bar{p}p\to\gamma\gamma$ with the η_c' may distort the line shape of the resonance. This effect was not considered in this analysis since neither the $\gamma\gamma$ cross section nor its partial amplitudes are known. We do not expect interference to alter the results of this analysis.

We obtain upper limits to the product $Br(\eta_c' \to \bar{p}p) \times Br(\eta_c' \to \gamma\gamma)$ anywhere in the search range as follows.

A maximum likelihood analysis of the data in the interval $3526 < \sqrt{s} < 3686$ MeV, which includes the background points at 3526 and 3686 MeV, was performed by fitting to a superposition of a Breit-Wigner resonance and a smooth background parametrized according to Eq. (3).

The likelihood function to be maximized, L, is written as the product of N (=number of data points in the energy scan) Poisson functions, each giving, for the ith data point, the probability that n_i events be observed if ν_i are expected,

$$L = \prod_{i=1}^{N} \frac{\nu_i^{n_i} e^{-\nu_i}}{n_i!}, \tag{4}$$

where

$$\nu_i = \left[\int \mathcal{L}\, dt \right]_i \left(\alpha \int f_i(\sqrt{s})\, \sigma_{peak} \times \frac{\Gamma^2}{4(\sqrt{s} - Mc^2)^2 + \Gamma^2} d\sqrt{s} + \sigma_{bkgd}(s) \right) (\epsilon_{\gamma\gamma})_i, \tag{5}$$

$$\sigma_{peak} = \frac{4\pi(\hbar c)^2(2J+1)}{s - 4m^2c^4} \times Br(\eta_c' \to \bar{p}p) \times Br(\eta_c' \to \gamma\gamma). \tag{6}$$

The integral gives the convolution of the resonance Breit-Wigner with the (Gaussian) center of mass energy distribution function $f_i(\sqrt{s})$, $\int \mathcal{L}\, dt$ is the integrated luminosity of each data point, α is the geometrical acceptance, M and Γ are the resonance mass and width, $\epsilon_{\gamma\gamma}$ is the efficiency given by formula (2), and m is the proton mass.

Repeated fits were performed, over a grid of fixed values of the resonance mass and width, covering the range 3575 to 3660 MeV/c^2 with three hypothetical values of the resonance width, 5, 10, and 15 MeV, in steps of 0.5, 1.0, and 1.0 MeV, respectively. Free parameters in the fits were the resonance branching ratio product $BR \equiv Br(\eta_c' \to \bar{p}p) \times Br(\eta_c' \to \gamma\gamma) \times 10^8$, and the background parameters A and B.

Several methods exist to produce limits when the signal being sought is small compared to the background and the parameter being measured has physical bounds [16]. In Appendix A we present a comparison of the upper limits obtained applying different methods to analyze this experiment.

In this section we present the method of Feldman and Cousins [17] applied assuming the best fit value to be Gaussian distributed with standard deviation equal to the parabolic error.[6] We calculate the 90% C.L. upper limit interpolating Table X of Ref. [17].

Since the upper limits tend to be underestimated when there are downwards fluctuations of the background, following the authors' suggestion we evaluated the sensitivity of our experiment [17]. The sensitivity is defined as the mean upper limit that would be obtained in repeated experiments under the same conditions with the same expected background but no true signal. The calculation of the experiment sensitivity is discussed in Appendix B.

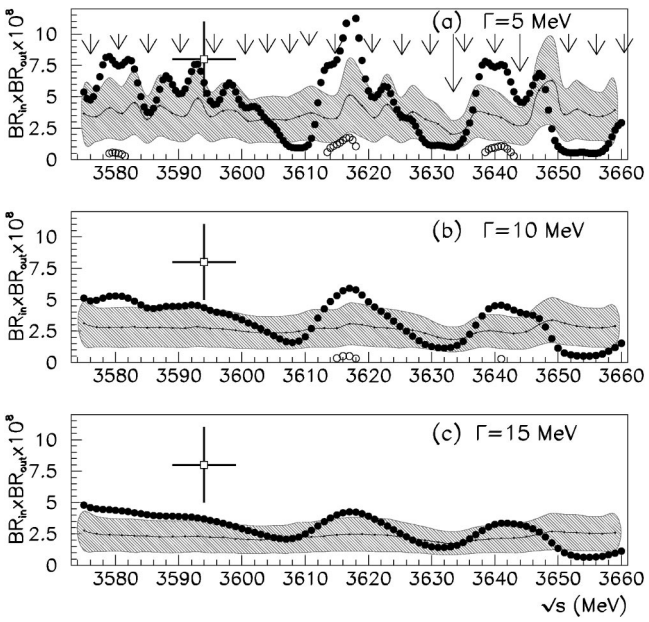

FIG. 4. 90% confidence intervals for the product of the $\bar{p}p$ and the $\gamma\gamma$ branching ratios vs $\sqrt{s}$. Full circles for upper limits; open circles for lower limits (not shown when zero). The resonance width was fixed at (a) 5 MeV, (b) 10 MeV, and (c) 15 MeV. The line in the shaded band is the experiment sensitivity (see the text). Arrows indicate the energies where data points were taken; arrow lengths are proportional to integrated luminosities. An estimate of $Br(\eta_c' \to \bar{p}p) \times Br(\eta_c' \to \gamma\gamma)$ is shown as the small open square. We have drawn it at the crystal ball η_c' candidate mass, with the horizontal error bar reflecting the uncertainty in the candidate's mass.

The limits on $Br(\eta_c' \to \bar{p}p) \times Br(\eta_c' \to \gamma\gamma)$ and the sensitivity of the experiment are presented in Fig. 4; shown as open (full) circles are the lower (upper) limits of the 90% confidence intervals. The curve represents the sensitivity of this experiment and the band displays the standard deviation range of upper limits obtained from repeated experiments in the absence of a resonance; upper limits below the sensitivity of the experiment, such as those occurring at $\sqrt{s}$ near 3610, 3630, and 3655 MeV are not significant and are interpreted as downwards fluctuations of the background. Notice the energy behavior of both the upper limit and the sensitivity, much smoother for $\Gamma = 10{,}15$ MeV than for $\Gamma = 5$ MeV. This is because the spacing in energy of the data points ($\sim$5 MeV) is too large for a $\Gamma = 5$ MeV resonance search, giving rise to local minima just at the scan points (indicated by arrows).

We have examined the effect of the choice of the background form by comparing the upper limits obtained using our standard form and using forms linear (2 parameter) and quadratic (3 parameter) in $\sqrt{s}$. We find that our results are independent of the way the background is parametrized. Likewise we found that the systematic errors on the integrated luminosity and on the efficiency $\epsilon_{\gamma\gamma}$ have negligible effect on our results.

[6] A Monte Carlo simulation of repeated experiments has shown this assumption to be realistic, see Appendix B.

TABLE II. Maximum likelihood solution for $BR = Br(\eta_c' \to \bar{p}p) \times Br(\eta_c' \to \gamma\gamma)$ in units 10^{-8} (combined E835-E760 experiments).

$\sqrt{s}$ (MeV)	$\Gamma = 5$ MeV $\widehat{BR}$	$\Gamma = 10$ MeV $\widehat{BR}$	$\Gamma = 15$ MeV $\widehat{BR}$	$\sqrt{s}$ (MeV)	$\Gamma = 5$ MeV $\widehat{BR}$	$\Gamma = 10$ MeV $\widehat{BR}$	$\Gamma = 15$ MeV $\widehat{BR}$
3576	1.4 ± 2.0	1.8 ± 1.8	1.7 ± 1.6	3618	3.1 ± 2.2	1.7 ± 1.4	1.1 ± 1.1
3578	3.1 ± 2.6	2.0 ± 1.7	1.7 ± 1.5	3620	2.2 ± 1.7	1.7 ± 1.3	1.2 ± 1.2
3580	3.5 ± 2.4	2.2 ± 1.7	1.6 ± 1.4	3622	2.4 ± 1.9	1.6 ± 1.4	1.1 ± 1.2
3582	3.3 ± 2.7	1.9 ± 1.7	1.4 ± 1.4	3624	1.8 ± 2.2	1.2 ± 1.4	0.8 ± 1.2
3584	0.8 ± 2.3	1.2 ± 1.7	1.2 ± 1.4	3626	0.5 ± 1.9	0.4 ± 1.5	0.4 ± 1.2
3586	0.1 ± 2.1	0.8 ± 1.6	0.9 ± 1.3	3628	-1.4 ± 2.2	-0.4 ± 1.4	0.0 ± 1.2
3588	0.6 ± 2.5	0.6 ± 1.5	0.7 ± 1.3	3630	-1.8 ± 1.6	-0.8 ± 1.3	-0.3 ± 1.1
3590	0.4 ± 1.6	0.5 ± 1.4	0.6 ± 1.2	3632	-1.4 ± 1.4	-0.7 ± 1.1	-0.3 ± 1.1
3592	0.4 ± 2.0	0.6 ± 1.4	0.6 ± 1.2	3634	-0.9 ± 1.1	-0.4 ± 1.1	-0.1 ± 1.1
3594	0.8 ± 1.9	0.7 ± 1.4	0.6 ± 1.2	3636	0.2 ± 1.7	0.2 ± 1.2	0.3 ± 1.1
3596	0.8 ± 1.8	0.7 ± 1.4	0.6 ± 1.2	3638	3.4 ± 2.5	1.4 ± 1.4	0.9 ± 1.2
3598	1.5 ± 2.5	0.8 ± 1.5	0.5 ± 1.2	3640	3.9 ± 2.1	2.1 ± 1.5	1.3 ± 1.2
3600	1.1 ± 1.9	0.6 ± 1.4	0.4 ± 1.2	3642	3.6 ± 2.1	2.1 ± 1.4	1.3 ± 1.2
3602	0.8 ± 1.9	0.3 ± 1.4	0.1 ± 1.2	3644	1.9 ± 1.6	1.6 ± 1.4	1.1 ± 1.3
3604	0.0 ± 1.7	-0.2 ± 1.3	-0.2 ± 1.2	3646	1.9 ± 2.4	1.1 ± 1.6	0.7 ± 1.4
3606	-1.7 ± 1.9	-1.0 ± 1.3	-0.6 ± 1.2	3648	-1.1 ± 4.0	-0.4 ± 1.9	-0.2 ± 1.5
3608	-2.8 ± 1.5	-1.7 ± 1.3	-0.8 ± 1.2	3650	-4.3 ± 2.4	-2.5 ± 1.8	-1.5 ± 1.6
3610	-4.3 ± 1.6	-1.8 ± 1.4	-0.7 ± 1.2	3652	-3.7 ± 1.6	-3.3 ± 1.6	-2.4 ± 1.5
3612	-3.0 ± 1.8	-0.9 ± 1.3	-0.3 ± 1.2	3654	-5.9 ± 2.1	-3.6 ± 1.5	-2.7 ± 1.5
3614	0.9 ± 1.6	0.4 ± 1.3	0.3 ± 1.1	3656	-3.6 ± 1.5	-3.1 ± 1.5	-2.5 ± 1.4
3616	2.2 ± 1.7	1.2 ± 1.3	0.8 ± 1.1	3658	-3.3 ± 2.2	-2.2 ± 1.5	-2.0 ± 1.4

B. Combined E835-E760 results

Experiment E760 [12] searched for the η_c' in the restricted center of mass energy regions 3590–3595 and 3612–3621 MeV for a total integrated luminosity of 6 pb^{-1}. Of the 34 pb^{-1} collected by the present experiment, 15.8 pb^{-1} were devoted to the region 3575–3621 MeV. No signal was seen by either experiment and combining the data of the two experiments improves the upper limits in the region below 3621 MeV.

We used the E760 data from Table II of Ref. [12], with the trigger and analysis efficiency equal to 0.537, and the data of this experiment in a combined maximum likelihood fit. To accommodate the fact that the background level in E760 was different from the background level in E835, we introduced two additional parameters A' and B' (to describe the E760 background) in the fits to the combined data sets.[7] Fits were done with the maximum likelihood method described in the previous section, this time with five free parameters: $BR = Br(\eta_c' \to \bar{p}p) \times Br(\eta_c' \to \gamma\gamma) \times 10^8$, A, B, A', and B'. Everything else, the grids of mass and width and the calculation of the 90% Feldman and Cousins upper limits, was done in the same way as before. Table II displays the central values $\widehat{BR}$ of BR and their parabolic errors (σ), as given by the fits. They are the inputs to the calculation of the F-C upper limits. As can be seen $\widehat{BR}$ can be negative, because no bound is imposed in the fitting program. The effect on the upper limits of a systematic error on the product $\epsilon_{\gamma\gamma} \times \int \mathcal{L}\, dt$ (7% in the E760 data and $<4\%$ in the E835 data) was found to be negligible. In comparing the data from the two experiments in Fig. 3, notice that even if the cross sections are corrected for the respective trigger and analysis efficiencies, they can still be different because the two experiments do not have the same background level. Figure 5 shows the 90% confidence intervals as a function of the center of mass energy for (a) $\Gamma = 5$ MeV, (b) 10 MeV, and (c) 15 MeV: the open circles are the limits from the combined experiments; for comparison, the full squares are the limits for the E835 experiment alone. The improvement of the limits near 3590 and 3617 MeV is evident.

[7] A separate fit to a pure background hypothesis of the E760 data led to $A' = (15.6 \pm 1.4)$ pb and $B' = 12.3 \pm 7.5$ to be compared to $A = (18.2 \pm 0.6)$ pb and $B = 4.7 \pm 1.9$ from E835 alone. Both results are largely determined by the high statistics data points at $\sqrt{s} \sim 3526$ and 3686 MeV.

V. CONCLUSIONS

A. Limits on $Br(\eta_c' \to \bar{p}p) \times Br(\eta_c' \to \gamma\gamma)$

Theoretical predictions of the η_c' mass have been reported with values of 3.57 [18], 3.62 [19], and 3.67 GeV/c^2 [20]. Our search for η_c' formation through reaction 1 has shown no evidence of it in the mass interval 3575–3660 MeV/c^2. The experiment sets limits on the product of the branching ratios to $\bar{p}p$ and $\gamma\gamma$ that vary with the mass and the resonance width, never departing significantly from the experiment sensitivity. We set the overall limits (at 90% confidence level):

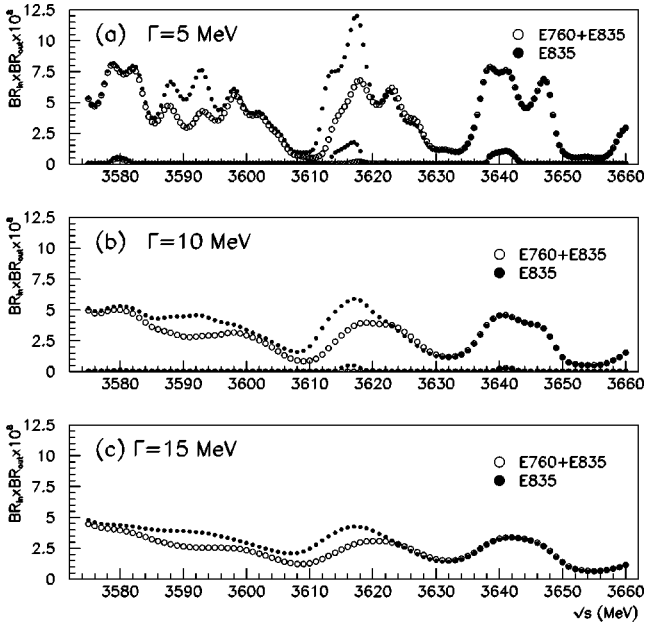

FIG. 5. 90% confidence intervals for the product of the $\bar{p}p$ and the $\gamma\gamma$ branching ratios vs $\sqrt{s}$. Open circles: the combined E760 and E835 experiments; full circles: the present experiment. The resonance width was fixed at (a) 5 MeV, (b) 10 MeV, and (c) 15 MeV. The lower limits of the confidence intervals for (c) are zero everywhere and have been omitted.

$$Br(\eta_c' \to \bar{p}p) \times Br(\eta_c' \to \gamma\gamma) < 12.0 \times 10^{-8} \ [\text{sensitivity } (5.1 \pm 2.9) \times 10^{-8}] \quad \text{for } \Gamma = 5 \text{ MeV},$$

$$Br(\eta_c' \to \bar{p}p) \times Br(\eta_c' \to \gamma\gamma) < 5.9 \times 10^{-8} \ [\text{sensitivity } (3.1 \pm 1.7) \times 10^{-8}] \quad \text{for } \Gamma = 10 \text{ MeV},$$

$$Br(\eta_c' \to \bar{p}p) \times Br(\eta_c' \to \gamma\gamma) < 4.8 \times 10^{-8} \ [\text{sensitivity } (2.8 \pm 1.5) \times 10^{-8}] \quad \text{for } \Gamma = 15 \text{ MeV}.$$

When the data of this experiment are combined with the data of E760, the upper limits become

$$8.0 \times 10^{-8} \text{ for } \Gamma = 5 \text{ MeV},$$

$$5.0 \times 10^{-8} \text{ for } \Gamma = 10 \text{ MeV},$$

and

$$4.5 \times 10^{-8} \text{ for } \Gamma = 15 \text{ MeV}.$$

The apparent excess near 3618 MeV [see Figs. 4(a) and 4(b)] occurs in the middle of a gap in the E835 scan and is highly damped when the E760 data are added to the E835 data (see Fig. 5).

B. Comparison with the Crystal Ball candidate

In the region (3594 ± 5 MeV/c^2) where the Crystal Ball reported a candidate with $\Gamma < 8$ MeV (95% CL), we set the following 90% confidence upper limits:

$$Br(\eta_c' \to \bar{p}p) \times Br(\eta_c' \to \gamma\gamma) < 7.6 \times 10^{-8} \ [\text{sensitivity } (4.2 \pm 2.4) \times 10^{-8}] \quad \text{for } \Gamma = 5 \text{ MeV},$$

$$Br(\eta_c' \to \bar{p}p) \times Br(\eta_c' \to \gamma\gamma) < 5.2 \times 10^{-8} \ [\text{sensitivity } (2.8 \pm 1.6) \times 10^{-8}] \quad \text{for } \Gamma = 8 \text{ MeV},$$

$$Br(\eta_c' \to \bar{p}p) \times Br(\eta_c' \to \gamma\gamma) < 4.6 \times 10^{-8} \ [\text{sensitivity } (2.3 \pm 1.3) \times 10^{-8}] \quad \text{for } \Gamma = 10 \text{ MeV}.$$

These limits become 5.6×10^{-8}, 3.7×10^{-8}, and 3.2×10^{-8}, respectively, when this experiment is combined with E760.

A direct comparison of our results with the findings of the Crystal Ball experiment [2] is not possible because of the different nature of the two experiments. The Crystal Ball signal was seen in the inclusive photon spectrum of ψ' decays and therefore does not depend on any decay branching ratio of the candidate η_c' while our investigation is tied to the unknown branching ratios of the candidate to $\bar{p}p$ and to $\gamma\gamma$.

To set a scale for a comparison, we assumed $Br(\eta_c' \to \gamma\gamma) = Br(\eta_c \to \gamma\gamma)$ and derived $Br(\eta_c' \to \bar{p}p)$ from $Br(\eta_c \to \bar{p}p)$ using a prescription given in Ref. [21] for the case of $J/\psi \to \bar{p}p$ and $\psi' \to \bar{p}p$. Details of this calculation are reported in Appendix C.

We obtain

$$[Br(\eta_c' \to \bar{p}p) \times Br(\eta_c' \to \gamma\gamma)] = (0.36 \pm 0.13) \times [Br(\eta_c \to \bar{p}p) \times Br(\eta_c \to \gamma\gamma)] = (8 \pm 3) \times 10^{-8}, \quad (7)$$

using $Br(\eta_c \to \bar{p}p) \times Br(\eta_c \to \gamma\gamma) = (22 \pm 4) \times 10^{-8}$ [13,22].

This estimate is compared to our experimental results in Figs. 3 and 4. We note that since $\bar{p}p \to \bar{c}c$ for the η_c and η_c' is suppressed by helicity conservation, it is possible that the rate for this process falls more rapidly with $\sqrt{s}$ than the corresponding rate for J/ψ and ψ'. Given the theoretical uncertainty in the derivation of the branching ratios, we conclude that our data do not rule out the existence of the Crystal Ball candidate.

C. Comparison with η_c

The η_c' has been searched for by other experiments [23,24]. DELPHI sets a limit on the ratio of the partial widths $\Gamma(\eta_c' \to \gamma\gamma)/\Gamma(\eta_c \to \gamma\gamma) \leqslant 0.34$ (90% C.L.), while L3 sets a limit of 2 keV (95% C.L.) for the η_c' partial width $\Gamma(\eta_c' \to \gamma\gamma)$. If we couple the result of our η_c' search with our η_c study, we can put the following 90% confidence limit:

$$\frac{Br(\eta_c' \to \bar{p}p) \times Br(\eta_c' \to \gamma\gamma)}{Br(\eta_c \to \bar{p}p) \times Br(\eta_c \to \gamma\gamma)} \leqslant \frac{8}{22} \leqslant 0.37 \qquad (8)$$

for a resonance of width $\geqslant 5$ MeV anywhere in the region 3575–3660 MeV (here we use the combined E760-E835 results for η_c' and E835 for η_c [13,22]). If we assume the $\gamma\gamma$ branching ratios of the η_c' and of the η_c to be the same (see Appendix C), we set a 90% confidence limit on the ratio of the $\bar{p}p$ branching ratios:

$$\frac{Br(\eta_c' \to \bar{p}p)}{Br(\eta_c \to \bar{p}p)} \leqslant 0.37. \qquad (9)$$

D. Comment on technique and prospects for the future

The limitation of the technique used in the present experiment is the relatively high level of background from $\pi^0\pi^0$ and $\pi^0\gamma$ compared to a $\gamma\gamma$ signal smaller than that expected at the time the experiment was proposed. Pursuing this search in the same channel with increased statistics may prove very hard unless the background level is substantially reduced. This would require new calorimetry, i.e., a newly designed experiment (lower energy threshold, improved angular and/or energy resolution and increased geometric acceptance).

A systematic η_c' search in exclusive radiative decays of the ψ' (3686) formed at e^+e^- machines may be decisive in confirming this resonance.

ACKNOWLEDGMENTS

The authors gratefully acknowledge the technical support provided by the Fermilab Research Division, Computing Division, Physics Section and Beams Division. They also thank the staff, engineers, and technicians at their respective institutions for their help and cooperation. This research was supported by the U.S. Department of Energy and the Italian Istituto Nazionale di Fisica Nucleare.

APPENDIX A: COMPARISON OF CLASSICAL, BAYESIAN AND FELDMAN-COUSINS UPPER LIMITS

The upper limits to BR, the product of the branching ratios of the η_c', have been calculated from the data of this experiment using three methods:

(a) The classical frequentist method with unbound parameter: the upper limit of the 90% two-sided confidence *interval* is calculated as $\widehat{BR} + 1.645\sigma$, where $\widehat{BR}$ is the best fit value and σ is the parabolic error given by the fitting program [25]; since the parameter is unbound, occasionally the upper limit can assume unphysical values, i.e., be negative in our case.

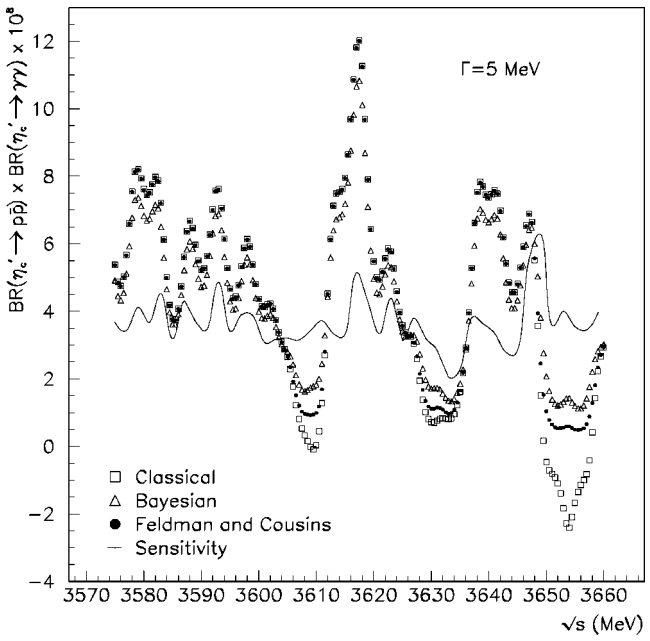

FIG. 6. The upper limits for $\Gamma(\eta_c') = 5$ MeV calculated with the classical Neyman method ignoring the physical bound, are compared to the limits calculated with a Bayesian method with physical bound at zero, and with the Feldman and Cousins method (see the text). The wavy line is the experiment sensitivity (see the text).

(b) A Bayesian approach assuming a prior ''probability'' of the unknown parameter BR flat in the physical region $BR > 0$ and null in the unphysical region $BR < 0$. Here the 90% confidence *limit* was considered, which in this method implies including 90% of the area above the bound to define the upper limit.

(c) The unified approach of Feldman and Cousins [17]. We give the 90% confidence *interval*.

A comparison of the results of the three methods for $\Gamma = 5$ MeV is shown in Fig. 6. One sees that the classical method produces negative limits near 3610 and 3655 MeV. In these regions and around 3630 MeV the Bayesian and the Feldman and Cousins methods give limits above the classical; the Bayesian limits are here more conservative than those of Feldman and Cousins. Elsewhere the first and last methods lead to almost identical results, while the Bayesian limits fall approximately 10% below the others; this is no surprise, since, away from the bound, the upper limit of a classical 90% two-sided confidence interval asymptotically corresponds to the Bayesian upper limit of a 95% one-sided confidence interval.

APPENDIX B: SENSITIVITY OF THE η_c' SEARCH

To calculate the sensitivity of the experiment, simulated experiments were generated under the hypothesis of a pure background with cross section parametrized according to Eq. (3) with $A = 18$ pb and $B = 6.2$. A grid of 43 M values from 3575 to 3659 MeV/c^2 (2 MeV/c^2 steps) times three values

of the total width ($\Gamma = 5$,10, and 15 MeV) was explored. For each pair of values of M and Γ, 2500 experiments were simulated, using the energy settings,[8] luminosities, analysis, and geometrical efficiencies of the actual experiment to generate the (Poisson distributed) number of events ''observed.'' For each of the simulations ($2500 \times 43 \times 3 = 322\,500$) a maximum likelihood fit was performed to a sum of background and of a spin zero Breit-Wigner resonance. Free parameters of the fit were the product $BR = Br(\eta_c' \to \bar{p}p) \times Br(\eta_c' \to \gamma\gamma) \times 10^8$ and the background parameters A and B.

The best fit parameters BR, A, and B have approximately Gaussian distributions with standard deviations close to the average parabolic error calculated from MINUIT.

For any given experiment i, BR_i and its parabolic error dBR_i are used to calculate the 90% C.L. upper limit $UPBR_i$, with the method of Feldman and Cousins: this is done for a Gaussian distributed BR_i, by interpolation of Table X of Ref. [17].

The average over 2500 experiments of $UPBR_i$ is taken as the sensitivity of the experiment for the particular mass and width. The shaded bands in Fig. 4 represent the sensitivity of the experiment as a function of the resonance mass.[9]

APPENDIX C: ESTIMATE OF THE $\bar{p}p$ AND $\gamma\gamma$ BRANCHING RATIOS OF THE η_c'

We assume the $\gamma\gamma$ branching ratio of the η_c' to be equal to that of η_c. This follows simply from the assumption that the decay of each of these states is predominantly through the $\bar{c}c$ annihilation into two gluons,[10] and the ratio of the rate into $\gamma\gamma$ to that into two gluons is determined essentially by the ratio of the electromagnetic fine structure constant α to the QCD coupling α_s [26]. Notice that this assumes that the large radiative QCD corrections present in the individual $\gamma\gamma$ and gluon-gluon rates may be expected to cancel out, when taking the ratio of branching ratios [26].

We relate the $\eta_c' \to \bar{p}p$ branching ratio to the known $\eta_c \to \bar{p}p$ branching ratio using ψ' and J/ψ data as follows.

Following Brodsky and Lepage [21], we use the ratio of ratios

$$rr = \frac{\dfrac{\Gamma(\psi' \to \bar{p}p)}{\Gamma(\psi' \to \text{light quark hadrons})}}{\dfrac{\Gamma(J/\psi \to \bar{p}p)}{\Gamma(J/\psi \to \text{light quark hadrons})}} \tag{C1}$$

that can be rewritten as

$$rr = \frac{Br(\psi' \to \bar{p}p)}{Br(J/\psi \to \bar{p}p)} \times \frac{Br(J/\psi \to \text{light quark hadrons})}{Br(\psi' \to \text{light quark hadrons})}. \tag{C2}$$

Inserting the experimental values [1]:

$$Br(J/\psi \to \bar{p}p) = (2.12 \pm 0.10) \times 10^{-3},$$

$$Br(\psi' \to \bar{p}p) = (1.9 \pm 0.5) \times 10^{-4},$$

$$Br(J/\psi \to \text{light quark hadrons}) = (69.4 \pm 2.1)\%,$$

$$Br(\psi' \to \text{light quark hadrons}) = (17.1 \pm 4.0)\%$$

we obtain

$$rr = 0.36 \pm 0.13.$$

We assume, for the η_c, η_c' states, that the ratio rr scales with mass in the same way it does for the ψ, ψ' states, and hence has approximately the same value. With the already mentioned assumption that the annihilation into two gluons dominates the decay of the η_c, η_c' states, we approximate $\Gamma = \Gamma_{light\ quark\ had.}$, and finally obtain

$$Br(\eta_c' \to \bar{p}p) = (0.36 \pm 0.13) Br(\eta_c \to \bar{p}p).$$

The error quoted is only statistical.

[8] Energy settings include the high statistics background points near the h_c and the ψ' formation energies, for a total of 64 data points and 61 degrees of freedom in a 3-parameter likelihood fit.

[9] The error of the average is of the order of a few percent; the band covers the rms variation of the upper limits over the ensemble of simulated experiments.

[10] The η_c cannot decay into $(\bar{c}c)$ states because of energy conservation, thus its decay is dominated by 2 gluon annihilation. The η_c' can decay to $(\bar{c}c)$ (e.g., strongly to $\eta_c\,2\pi$ or electromagnetically to $h_c + \gamma$), however the partial rates of these processes are negligible compared to the 2 gluon rate [27].

[1] Particle Data Group, D.E. Groom *et al.*, Eur. Phys. J. C **15**, 1 (2000).

[2] C. Edwards *et al.*, Phys. Rev. Lett. **48**, 70 (1982).

[3] M. Church and J. Marriner, Annu. Rev. Nucl. Part. Sci. **43**, 253 (1993).

[4] D. Allspach *et al.*, Nucl. Instrum. Methods Phys. Res. A **410**, 195 (1998).

[5] S. Bagnasco *et al.*, Nucl. Instrum. Methods Phys. Res. A **409**, 75 (1998).

[6] M. Ambrogiani *et al.*, Nucl. Instrum. Methods Phys. Res. A **419**, 632 (1998).

[7] S. Bagnasco *et al.*, Nucl. Instrum. Methods Phys. Res. A **424**, 304 (1999).

[8] L. Bartoszek *et al.*, Nucl. Instrum. Methods Phys. Res. A **301**,

47 (1991).
[9] S. Trokenheim *et al.*, Nucl. Instrum. Methods Phys. Res. A **355**, 308 (1995).
[10] G. Oleynik *et al.*, IEEE Trans. Nucl. Sci. **44**, 460 (1997).
[11] R. Ray *et al.*, Nucl. Instrum. Methods Phys. Res. A **307**, 254 (1991).
[12] T.A. Armstrong *et al.*, Phys. Rev. D **52**, 4839 (1995).
[13] M. Stancari, Ph.D. thesis, University of California, Irvine, 1999.
[14] O. Dahl, T. Day, and F. Solmitz, Technical Report No. P-126, University of California, Lawrence Radiation Laboratory, 1965.
[15] M. Ambrogiani *et al.*, Phys. Rev. D **62**, 052002 (2000).
[16] Proceedings of the Workshop on Confidence Limits, CERN, Geneva, Switzerland, 2000, CERN 2000-005.
[17] G.J. Feldman and R.D. Cousins, Phys. Rev. D **57**, 3873 (1998).
[18] R.K. Bhaduri, L.E. Cohler, and Y. Nogami, Nuovo Cimento A **65**, 376 (1981).
[19] S. Godfrey and N. Isgur, Phys. Rev. D **32**, 189 (1985).
[20] J. Resag and C.R. Münz, Nucl. Phys. A **590**, 735 (1995).
[21] S.J. Brodsky and G.P. Lepage, Phys. Rev. D **24**, 2848 (1981).
[22] T.K. Pedlar, Ph.D. thesis, Northwestern University, Evanston, 1999.
[23] DELPHI Collaboration, P. Abreu *et al.*, Phys. Lett. B **441**, 479 (1998).
[24] L3 Collaboration, M. Acciarri *et al.*, Phys. Lett. B **461**, 155 (1999).
[25] F. James, MINUIT-Function Minimization and Error Analysis, CERN Program Library entry D506.
[26] W. Kwong and P.B. Mackenzie, Phys. Rev. D **37**, 3210 (1988).
[27] W. Kwong, J.L. Rosner, and C. Quigg, Annu. Rev. Nucl. Part. Sci. **37**, 325 (1987): see p. 352.